IF-UFRJ-92-33

INSTITUTO DE FÍSICA - UFRJ

Fermilab Library
0 1160 0017943 6

IF/UFRJ/92/33

14

FERMI
JUL 27 1993
LIBRARY

SEMICLASSICAL TREATMENT OF NUCLEAR REACTIONS

L.F. Canto

Dez/92

UNIVERSIDADE FEDERAL DO RIO DE JANEIRO
INSTITUTO DE FÍSICA
Cx. P. 68.528
21.944 - RIO DE JANEIRO
BRASIL

Semiclassical Treatment of Nuclear Reactions*

L.F. Canto
Instituto de Física, Universidade Federal do Rio de Janeiro
C.P. 68528, 21945 Rio de Janeiro, RJ, Brazil

December 14, 1992 Rio de Janeiro U

Abstract

We discuss nuclear reactions involving a large number of strongly coupled channels. In such cases, the coupled differential equations describing the collision dynamics become prohibitively complicated and one has to resort to approximate treatments. One of these treatments is the Alder and Winther's classical trajectory method, developed to study Coulomb excitation of collective states in heavy ion collisions at sub-barrier energies. In this talk I discuss the generalization of this method so as to include nuclear effects and its use in the description of other nuclear reactions. Special attention is payed to pair transfer reactions in deformed nuclei and to the Coulomb dissociation of neutron-rich nuclei.

1 Introduction

As it is well known, nuclei are highly complicated quantum mechanical systems of many interacting particles and their dynamics cannot be determined exactly. It is necessary, therefore, to develop approximate nuclear models. Typically, these models take into account a set of degrees of freedom, generically represented by ξ, and the stationary states of the system, $\varphi_i(\xi)$, are determined through the solution of a Schödinger equation with a model hamiltonian h,

15th

*an invited talk presented at the 'XV Workshop on Nuclear Physics', 14 to 18 september 1992, Buenos Aires, Argentina

MN

$$h\ \varphi_i(\xi) = \varepsilon_i\ \varphi_i(\xi)\ . \tag{1}$$

To test the validity of the model, one has to compare its predictions with corresponding experimental results. This is usually done in nuclear reactions, where the cross section for observable quantities are related to final states populated in the collision. Neglecting intrinsic degrees of freedom of one of the collision partners, the hamiltonian of the projectile-target system has the general form

$$H = H_{opt}(\mathbf{r}) + h + V(\mathbf{r};\xi)\ , \tag{2}$$

where $H_{opt}(\mathbf{r})$ is the optical hamiltonian, which depends exclusively on the projectile-target separation $\mathbf{r}$, h is the intrinsic hamiltonian of eq. (1) and $V(\mathbf{r};\xi)$ is the coupling potential. Since the cross sections depend on the matrix elements $<\varphi_i|V(\mathbf{r};\xi)|\varphi_j>$, the comparison with experiment tests the validity of the model.

However, to express the cross sections in terms of the matrix elements of the coupling, it is necessary to solve the coupled Schrödinger equations in the multi-channel space. In principle, this problem can be handled by coupled-channels codes. However, when the number of relevant channels is large, such codes demand gigantic computer power. This is the case, for example, of collisions of very heavy projectiles with deformed target nuclei, where the strong coulomb field excites many rotational states. Under these circumstances, the use of standard coupled-channels codes becomes unpractical and the collision dynamics should be treated within approximations.

2 The classical trajectory approximation to the coupled-channels problem

In heavy ion collisions at energies near or above the Coulomb barrier, the wavelength associated to the projectile-target separation is much smaller than the characteristic lengths of the potentials in the hamiltonian of eq. (2). It is, therefore, a reasonable approximation to treat $\mathbf{r}$ as a classical variable $\mathbf{r}(t)$, given at each instant by the trajectory followed by the relative motion. The intrinsic dynamics can then be handled as a quantum mechanics problem with a time dependent hamiltonian. This treatment was first developed by Alder and Winther [1] to study Coulomb excitation of collective states in heavy ion collisions.

The intrinsic wave function $\psi(\xi,t)$ satisfies the Schrödinger equation

$$[h\ +\ V(\mathbf{r}(t),\xi)]\ \psi(\xi,t) = i\hbar\frac{\partial\psi(\xi,t)}{\partial t}\ . \tag{3}$$

Expanding the wave function in a set of eigenstates of h,

$$\psi(\xi,t) = \sum_{m=0}^{N} a_m(t)\, \varphi_m(\xi)\, \exp^{-i\varepsilon_m t/\hbar}\,, \tag{4}$$

where N should be large enough as to guarantee convergence, and taking scalar product with each of orthonormal states $< \varphi_n|$, we get the set of coupled equations

$$-\,i\hbar\, \dot{a}_n(t) = \sum_{m=0}^{N} < \varphi_n|V|\varphi_m >\, e^{i(\varepsilon_n-\varepsilon_m)t/\hbar}\, a_m(t) \qquad n = 0 \text{ to } N\,. \tag{5}$$

It should be remarked that the amplitudes depend also on the impact parameter b specifying the classical trajectory followed by the system. For the sake of keeping the notation simple, we do not indicate this dependence explicitly. We write, therefore, $a_n(t)$ instead of $a_n(b,t)$. Since the interaction V vanishes as $t \to \pm\infty$, the amplitudes have as initial condition $a_n(t \to -\infty) = \delta(n,0)$ and they tend to constant values as $t \to \infty$. Therefore, the excitation probabity of an intrinsic state φ_n in a collision with impact parameter b is given as

$$P_n(b) = |a_n(\infty)|^2\,. \tag{6}$$

The total cross section for excitation of the state n can be approximated by the classical expression

$$\sigma_n = 2\pi \int P_n(b)\; b db\,. \tag{7}$$

The differential cross section can, similarly, be approximated as

$$\frac{d\sigma_n(\theta)}{d\Omega} = P_n(b_\theta)\, \left(\frac{d\sigma(\theta)}{d\Omega}\right)_{Rutherford}\,. \tag{8}$$

Above, b_θ is the impact parameter for a trajectory emerging with an angle θ.

The set of coupled equations in (5) is much simpler than the exact coupled-channels equations, since they are of first order and involve a single variable.

3 Applications

As we mentioned in the previous section, Alder and Winther [1] used the classical trajectory method to study Coulomb excitation. In their works $\mathbf{r}(t)$ are Rutherford trajectories, φ_n are rotational or vibrational states and $V(\mathbf{r},\xi)$ is the electromagnetic

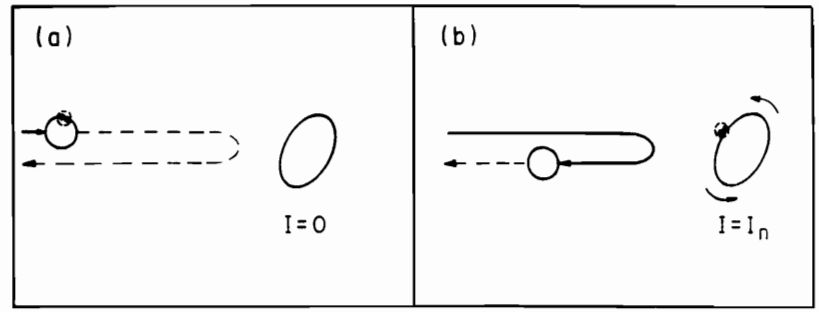

Figure 1: The transfer of a nucleon pair from a spherical to a deformed nucleus. Along the collision the deformed nucleus acquires a nucleon pair and I_n units of angular momentum

coupling. More recently, this method has been extended to study Coulomb-nuclear interference in the excitation of rotational states [2], to the transfer of one [3] or two nucleons [4, 5, 6, 7, 8] and to the break-up of neutron-rich projectiles [9, 10]. The method has also been improved as to include distortions of the Rutherford trajectory arising from the nuclear field and to take into account absorption effects [2]. In the next subsections we will discuss two of these applications, emphasizing the results of some very recent work.

3.1 Diabolic pair transfer in rotating nuclei

Let us consider the transfer of a nucleon pair in a sub-barrier energy collision of a spherical projectile with a deformed even-even target, as represented in figure 1. To keep the calculation simple, we restrict the study to head-on collisions, setting $b = 0$. The practical consequence of this restriction is that the theoretical predictions should be compared to data at backward angles. As the projectile approaches the target (figure 1a), the multipoles of the deformed Coulomb and nuclear fields induce rotations of the target and its angular momentum changes from the initial value $I = 0$ to a distribution over various I-values. At closer separations a neutron pair is transfered from the spherical to the deformed collision partner, as indicated in figure 1b.

The intrinsic states of the target can be writen [1] as $|\varphi_n >= |I_n, A_n >$, in terms of the total angular momentum and the number of nucleons. These states can be

[1] For simplicity, we omit other quantum numbers since they do not play an important role in the example under discussion

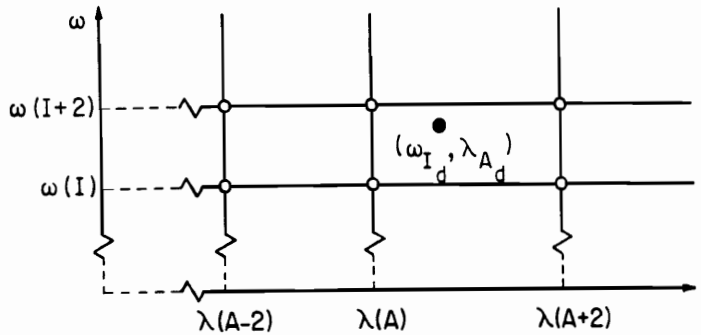

Figure 2: Schematic representation of a region on the plane $\omega - \lambda$. The points giving rise to physical states are indicated by open circles. A diabolical point (solid circle) between the lines for A and $A+2$ and the lines for I and $I+2$ is located at the point $(\omega_{I_d}, \lambda_{A_d})$.

grouped into two sets. A set with $A_n = A_0$, the initial mass number of the target, which we will call A, and the set of transfer channels, with $A_n = A+2$. The matrix-elements of the semiclassical coupled equations (eq. (5)) can be approximated as

$$< I_n, A+2|V|I_m, A > \approx F(t) \cdot S(I_n) \cdot \delta(I_n, I_m) \ , \tag{9}$$

where $S(I_n)$ are the pair transfer matrix elements

$$S(I_n) = < I_n, A+2| \left(a^\dagger a^\dagger\right)_0 |I_n, A > \ . \tag{10}$$

Above, $\left(a^\dagger a^\dagger\right)_0$ creates a neutron pair with spin 0 on the target. The time dependent factor has been discussed in details in reference [4] (see also ref. [8]). It contains the information of the tunnelling factor and of the classical trajectory followed by the system.

A very interesting effect can be predicted when one uses realistic microscopic descriptions, like the Cranked Hartree-Fock-Bogoliubov (CHFB), to obtain the target states. In this method, the many-body states are writen $|I_n, A_n >= |\omega(I_n), \lambda(A_n) >$, in terms of the Lagrange multipliers ω and λ, chosen as to guarantee that the target has average angular momentum I_n and average particle number A_n. It is interesting to consider the states generated by different values of the Lagrange multipliers. If we represent ω on the x-axis, λ on the y-axis and the energy of the states on the z-axis, the rotational energies form surfaces. The Yrast states correspond to the lowest surface, the Yrare are next and so on. For some special points on the $\omega - \lambda$ plane two of such surfaces may touch. This situation has been studied by several authors [11, 12]. Teller [12] showed that at these degeneracy points the two surfaces

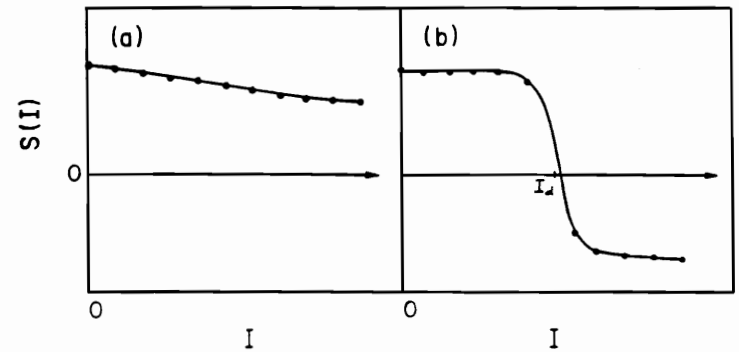

Figure 3: The pair transfer matrix element as a function of the angular momentum. In a) there is no diabolical point involved and $S(I)$ changes smoothly with I. In b) a diabolical point at I_d produces a sign change.

are connected as two sheets of a double cone: a diabolo, and, to stress this conical geometry, Berry and Wilkinson [11] gave them the name of "diabolical points".

One should have in mind, however, that only a discrete set of points on the $\omega - \lambda$ plane leads to physical states. The points leading to a given even integer I_n-value describe a continuous line on this plane and the same happens with respect to a mass number A_n. The physical states are generated by the points where these lines (one for I and one for A) intersect. This situation is depicted in figure 2, for a few values of the mass number and the angular momentum. A pair transfer corresponds to a transition from some point on the line for a mass number A_n to the line for $A_n + 2$. If the pair does not carry angular momentum, the transition keeps the system on the same angular momentum line.

The pair-transfer matrix elements $S(I_n)$ have been investigated by Nikam *et al.* [13] and these authors have shown that they depend strongly on the position of diabolical points on the $\omega - \lambda$ plane. If one considers the situation of figure 2, a transition from the line for mass number $A-2$ to mass number A does not involves a diabolical point while the transition from A to $A+2$ does. As a consequence, the pair transfer matrix elements show a qualitatively different behavior in each case. In the former, they change smoothly with I as is sketched in figure 3a. In the latter, they change sign as the angular momentum goes through the value I_d associated to the diabolic point, as indicated in figure 3b.

A sign change in $S(I)$ is expected to have important consequences on the spin distribution of the pair transfer cross section. Qualitatively, this can be understood from figure 4, where two possible transfer paths, a and b, leading to the same final spin I_f are represented. In a, the target undergoes Coulomb excitation until it reaches

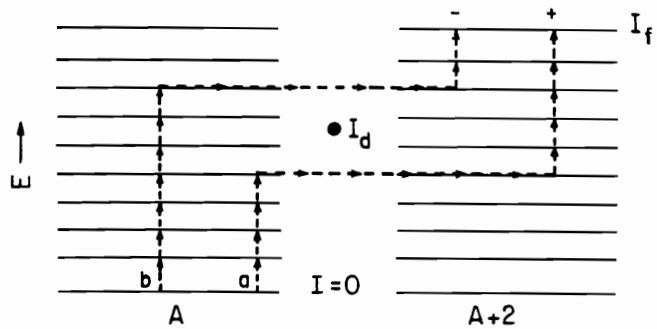

Figure 4: Schematic representation of two paths leading to pair transfer to the same final angular momentum I_f. In a the transfer occurs at an angular momentum below that of the diabolical point I_d. In b it occurs above I_d. The resulting amplitudes have opposite signs in each case.

some angular momentum below I_d, increases its mass by two units through the capture of a pair and then reaches the final angular momentum I_f through subsequent Coulomb excitation. In b, the system evolves in a similar way, with the difference that the pair transfer occurs at an angular momentum above I_d. Since the pair transfer matrix elements have opposite signs in each case, one expects that the contributions from these paths interfere destructively, leading to suppression of the transfer cross section to high (above I_d) spins. This suppression is usually called diabolical pair transfer.

A quantitative study of diabolical pair transfer has been carried out [4] (see also ref. [5]) in collisions of ^{208}Pb with the deformed nuclei ^{158}Dy and ^{160}Dy. CHFB calculations indicate a diabolical point between the lines for $A = 160$ and $A = 162$, at I_d between 10 and 12, and no diabolical point between $A = 158$ and $A = 160$. Therefore, one expects suppression of high spins in the pair transfer reaction $^{208}Pb +^{160} Dy \rightarrow^{206} Pb +^{162} Dy$. The results are shown in figure 5. In a) the pair transfer is diabolical and in b) it is not. Indeed, one can observe suppression even at angular momenta as low as $I = 6$.

The above discussion has been restricted to pair transfer between Yrast states. Dasso and Winther [6] has shown that the consideration of Yrare states may lead to drastic changes in the diabolical transfer signature of figure 5. For each spin I, these authors write the Yrast and the Yrare states as combinations of states of the g- and s-bands and obtain the coefficients by diagonalization of the target hamiltonian with a band mixing term v. This term is assumed to be very weak ($v \approx 0.05 - 0.10$ MeV) and I-independent, and the diabolical effect is introduced through the use of opposite signs for the initial and final nuclei. The Yrast states are very similar to

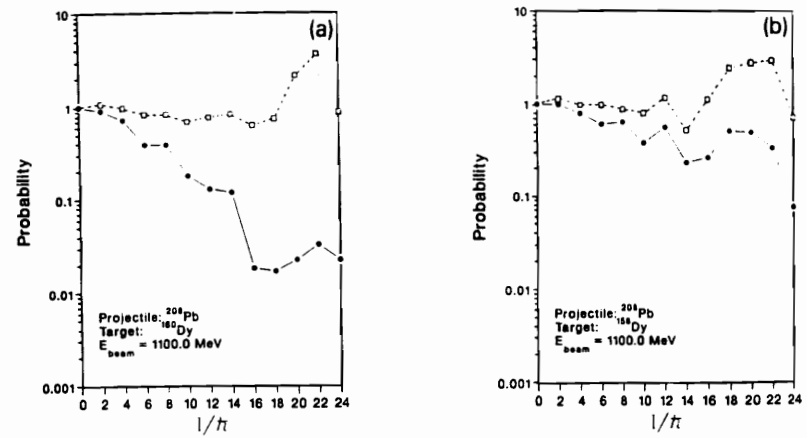

Figure 5: Spin distributions after pair transfer from ^{208}Pb at $E_{lab} = 1100$ MeV (solid circles). In a) the target is ^{160}Dy and in b) the target is ^{158}Dy. As a reference the spin distribution for Coulomb excitation is indicated by open squares, in each case.

g-band states below level-crossing and to s-band states above level-crossing. Since neither the inelastic nor the transfer couplings leads to transitions from states of the g-band to states of the s-band (for a discussion of this point we refer to [8]), the population of yrast states with $I > I_d$ is always very weak, independently of the diabolical effect. Therefore, the experimental identification of diabolical transfer becomes much harder.

Recently, the role of the band-mixing strength in the signature of diabolical transfer has been investigated [7]. Microscopic calculations [14] indicate that the mixing strength can be considerably stronger than the values used in ref. [6] for some heavy rare earths midway between diabolical points. This would be the case of ^{172}Hf, ^{174}Hf and ^{176}Hf, for which the mixing strengths are in the range 0.2 to 0.3 MeV. The calculation of Sun *et al.* [14] predicts a diabolical point near $I = 14$ between $A = 172$ and $A = 174$. A comparison between the spin distributions for stripping and the pick-up of a neutron pair in collisions of ^{174}Hf with heavy projetiles would offer ideal conditions for the search for a signature of diabolical transfer.

The results of such a calculation [7] for ^{206}Pb projectiles at $E_{cm} = 1000$ MeV appears in figure 6. The pick-up reaction (solid circles), leading to ^{172}Hf, is diabolical while the stripping reaction (open circles), leading to ^{176}Hf, is not. Figures 6a and 6b show, respectively, the spin distributions for pair transfer to Yrast and to Yrare states. We notice that in both cased there are pronounced differences between diabolical and non-diabolical transfer.

One concludes that the weak band mixing near diabolical points may pose se-

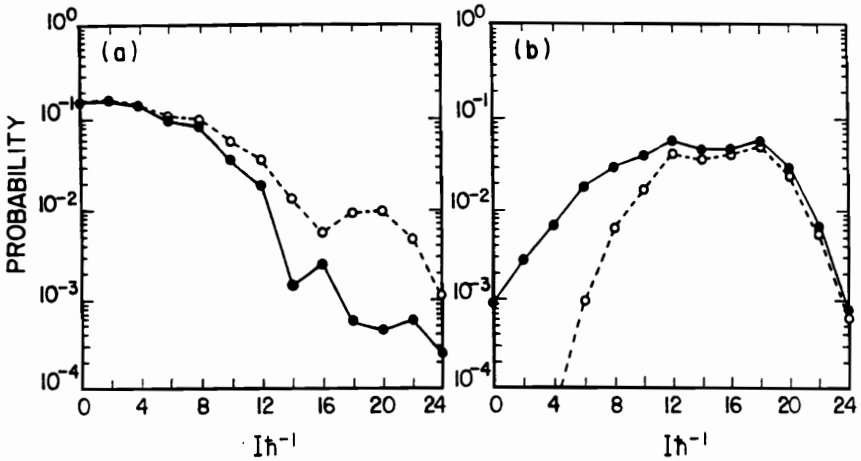

Figure 6: Diabolical (solid circles) and non-diabolical (open circles) pair transfers in ^{174}Hf in collisions with ^{206}Pb. In (a) the tranfer populates Yrast states and in (b) it populates Yrare states. For details see the text.

rious difficulties in the characterization of diabolical transfer. However, in some special cases, there remain appreciable differences between diabolical and non-diabolical transfers.

3.2 Coulomb dissociation of ^{11}Li

With the availability of radiactive beams, the interest in neutron-rich nuclei, like ^{11}Li, has grown considerably. In ^{11}Li, a neutron pair is very weakly bound to a ^{9}Li core ($E_B \simeq 0.2$ MeV) so that this pair forms a "halo", and its density spreads far beyond that expected for a normal 11 nucleon system. These characteristics lead to very large Coulomb dissociation cross sections in collisions with heavy targets. Therefore, the use of perturbative approaches to the reaction dynamics may be inappropriate and the semiclassical-coupled channels treatment of sect. 2 presents itself as a natural candidate. Investigations along this line have been carried out in refs. [9, 10] and their main results are summarized below.

A ^{11}Li collision with a heavy target is represented in figure 7. As one wants to use the projectile frame, the target approaches the projectile from the right. The separation between the centers of mass is given at each instant by the classical trajectory $\mathbf{r}(t)$. The relative coordinate between the neutron pair, treated as a cluster, and the ^{9}Li core is represented by the vector $\mathbf{x}$. The cluster is initially bound to the core but the interaction excites the system to a state in the continuum. The classical trajectory is approximated by a straight line with impact parameter b.

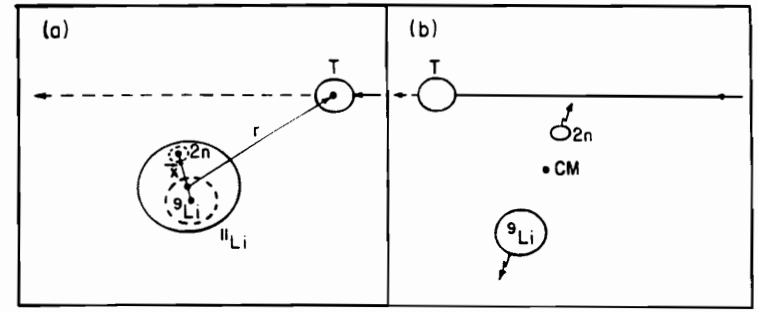

Figure 7: Representation of the ^{11}Li dissociation. T indicates the target, approaching the projectile from the left. For details see the text.

The intrinsic motion of the ^{9}Li+$2n$ system is described by the state

$$|\psi(t)> = a_0(t)\, e^{-i\varepsilon_0 t/\hbar}\, |\varphi_0> \; + |\psi_c(t)> , \tag{11}$$

where $\varphi_0(\mathbf{x})$ is the bound component

$$\varphi_0(\mathbf{x}) \approx \frac{\exp\left(-\sqrt{2\mu\varepsilon_0}\; x/\hbar\right)}{x}, \tag{12}$$

with $\varepsilon_0 = -E_B$, and $|\psi_c(t)>$ is the continuum component, which can be writen as a superposition of angular momentum projected free states $|\varepsilon lm>$. However, if one follows the procedure of sect. 2, one obtains an infinite set (and with a continuous label) of coupled differential equations, which cannot be solved. This difficulty can be avoided by the approximation of discretizing the continuum [9]. One replaces the basis of spherical waves by the finite set of wave packets

$$|\varphi_{jlm}> = e^{-i\varepsilon_j t/\hbar} \int \Gamma_j(\varepsilon)\; |\varepsilon lm> d\varepsilon \; . \tag{13}$$

The amplitudes $\Gamma_j(\varepsilon)$ have been discussed in details in ref. [9]. They are centered at the energies ε_j of a mesh covering the relevant range of fragment energies, their widths have the order of the mesh spacing, and they should satisfy the orthonormality relations

$$\int \Gamma_i(\varepsilon)\; \Gamma_j(\varepsilon)\; d\varepsilon = \delta(i,j) \tag{14}$$

The continuum component ψ_c can then be expanded as

$$|\psi_c(t)> = \sum_{jlm} a_{jlm}(t)\; e^{-i\varepsilon_j t/\hbar}\; |\varphi_{jlm}> \; . \tag{15}$$

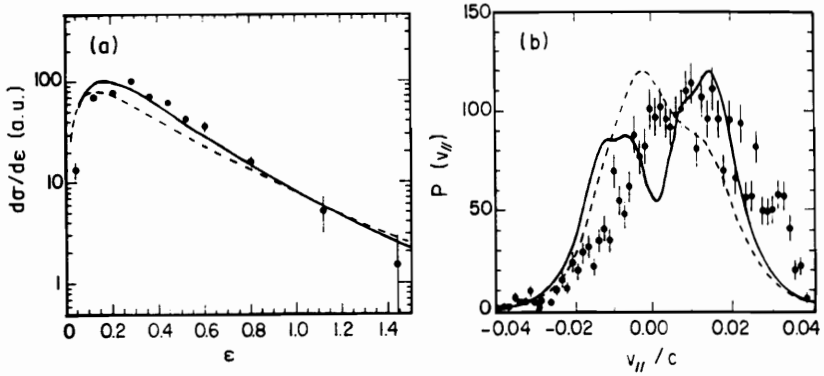

Figure 8: Energy (a) and longitudinal velocity (b) distributions in ^{11}Li dissociation. The solid and the dashed lines in (a) indicate the results of eq. (17) and of first order perturbation theory, respectively. The solid and dashed lines in (b) were obtained with eq. (19), using $\varepsilon_\perp^{max} = 15$ and 130 keV, respectively. In both cases the data are from ref. [15] and the results are given in arbitrary units.

The coupling potential is the electromagnetic interaction

$$V(\mathbf{x},t) = Z_T e^2 \left[\frac{Z_{Li}}{\sqrt{(y-b)^2 + (z - v_{beam}t)^2}} - \frac{Z_{Li}}{\sqrt{b^2 + v_{beam}^2 t^2}} \right], \tag{16}$$

which is treated within the dipole approximation.

Since the ^{9}Li+2n system is bound before the collision, the initial conditions for the coupled differential equations are $a_n(-\infty) = \delta(n,0)$, where n stands for quantum numbers jlm, specifying the states of the continuum set. The differential equations can be solved and from the final wave function one can make predictions for observable quantities.

In a very recent work, Ieki *et al.* [15] measured the energy spectrum of the fragments produced in the ^{11}Li break up, in its reference frame. They also measured the longitudinal component of the relative velocity ($\mathbf{v}_{^9Li} - \mathbf{v}_{2n}$) distribution. As it will be discussed below, their data plays an important role in the investigation of the dominating dissociation mechanism.

The semiclassical coupled-channels approximation leads to the prediction of an energy spectrum

$$P(\varepsilon) = 2\pi \sum_{lm} \int_{b_{min}}^{\infty} |< \varepsilon lm|\psi_c >|^2 \, b db \, . \tag{17}$$

The b-dependence of the integrand is contained in the coefficients a_{jlm} which defines ψ_c, according to eq. (15). The cut-off value b_{min} arises from nuclear absorption or

from the angular observation range of the experiment to which one wants to compare the theoretical distribution.

The longitudinal velocity distribution $P(v_\parallel)$ is a little more complicated. One should initially obtain the amplitudes

$$A(\mathbf{k},\mathbf{b}) \equiv A(\mathbf{k}_\perp, k_\parallel, \mathbf{b}) =< \mathbf{k}|\psi_c > , \tag{18}$$

distinguishing the longitudinal ($k_\parallel$) and the transverse ($\mathbf{k}_\perp$) components of $\mathbf{k}$, and then integrate $|A(\mathbf{k},\mathbf{b})|^2$ over the transverse momentum and impact parameter,

$$P(v_\parallel) \equiv P(\hbar k_\parallel/\mu) = (2\pi)^2 \int_{b_{min}}^{\infty} b\, db \int_0^{k_\perp^{max}} k_\perp \, dk_\perp \, |A(\mathbf{k},\mathbf{b})|^2 \, . \tag{19}$$

Above, the cut-off value $k_\perp^{max}$ is related to the transverse energy as

$$\varepsilon_\perp^{max} = (\hbar k_\perp^{max})^2/2\mu. \tag{20}$$

This quantity might be associated to the experimental detection angle, but its determination would require knowledge of the full kinematics of the three body system. For this reason $\varepsilon_\perp^{max}$ has been considered to be a parameter in ref. [10].

Figure 8a and b (from ref. [10]) shows a comparison between theoretical predictions and the data of Ieki *et al.* [15]. In a the experimental energy spectrum is compared to the spectrum of eq. (17) In b the experimental longitudinal velocity distribution is compared to the predictions of eq. (19). The theoretical energy distribution is in excelent agreement with the data. It is interesting to notice that this agreement depends on high order effects of the coupling. This is evident through the comparison with the theoretical prediction of first order perturbation theory, appearing in figure 8a as a dashed line. Neither it has the right slope nor it gives a reasonable description of the data near its maximum, at low energies. The agreement between the theoretical velocity distribution and the data is not as good as in the previous case. However, the theory is consistent with the main trends of the data, specially with respect to the shift of the centroid towards positive velocities. This agreement is noticeably better if one uses the transverse energy cut-off $\varepsilon_\perp^{max} = 130$ keV (solid line).

The shift to forward velocities has great importance to the determination of the reaction mechanism in the dissociation of ^{11}Li. It indicates a post-dissociation acceleration effect, suggesting that the dissociation occurs along the collision. In that case, the Coulomb forces acts on a lower mass (^{9}Li) during late stages of the collision, producing a larger positive acceleration. This result is a strong evidence against the hyphotesis that a long-lived soft mode plays an important role in the ^{11}Li dissociation and in favor of the direct mechanism adopted in refs. [9, 10].

4 Conclusions

We have discussed the problem of many coupled channels in nuclear reactions. The classical trajectory approximation of Alder and Winther [1] has been described and some applications have been considered. The diabolical pair transfer in rotating nuclei [4, 5, 6, 7, 8] and the Coulomb dissociation of ^{11}Li [9, 10] have been considered in detail. In the former, we have discussed the search for a diabolical effect signature in transfers to Yrast and to Yrare states. It has been argued that the consideration of Yrare states complicates the identification of the diabolical transfer [6], except for a few isolated cases [7] where the band mixing is strong [14]. In the latter, we described the approach of ref. [9] with the discretization of the continuum and discussed its application in the description of recent data of Ieki *et al.* [15]. It has been concluded that the success of the model and the shift of the longitudinal velocity distribution towards forward velocities indicates a direct process, rather than the excitation of a long-lived low lying soft mode.

This talk is based on research done in collaboration with C.A. Bertulani, S.Y. Chu, R. Donangelo, A.R. Farhan, M.W. Guidry, R.S. Nikam, J.O. Rasmussen, P. Ring, H. Schultz, Y. Sun and M.A. Stoyer. I acknowledge partial finantial support from the Brazilian National Research Council (CNPq) and the ICTP (Triestre).

References

[1] K. Alder and A. Winther, Electromagnetic Excitation (North Holland, Amsterdam, 1975); J. de Boer and A. Winther, in: Coulomb Excitation, eds. K. Alder and A. Winther (Academic Press, New York, 1966).

[2] L.F. Canto, R. Donangelo, J.O. Rasmussen, P. Ring and M.A. Stoyer, Phys. Lett. **B248** (1990) 10.

[3] J.O. Rasmussen, M.A. Stoyer, L.F. Canto, R. Donangelo and P. Ring, Z. Phys. **A339** (1991) 141.

[4] L.F. Canto, R. Donangelo, R.S. Nikam and P. Ring, Phys. Lett. **B192** (1987) 4; L.F. Canto, R. Donangelo, M.W. Guidry, A.R. Farhan, J.O. Rasmussen, P. Ring and M.A. Stoyer, Phys. Lett. **B241** (1990) 295.

[5] C. Price, H. Esbensen and S. Landowne, Phys. Lett. **B197** (1987) 15;J. de Boer, C.H. Dasso and G. Pollarolo, Z. Phys. **A335** (1990) 199.

[6] C.H. Dasso and A. Winther, Phys. Lett. **B242** (1990) 323.

[7] L.F. Canto, P. Ring, Y. Sun, J.O. Rasmussen, S.Y. Chu and M.A. Stoyer, submitted for publication in Phys. Rev. C

[8] M. Bernath, R.A. Broglia, Y.R. Shimizu, J.H. Sørensen and E. Vigezzi, submitted for publication in Nucl. Phys. A.

[9] C.A. Bertulani and L.F. Canto, Nucl. Phys. **A539** (1992) 163.

[10] L.F. Canto, R. Donangelo and H. Schultz, preprint NBI 92-91 and submitted for publication in Phys. Rev. C.

[11] M.V. Berry, Proc. R. Soc. Lond. **A392** (1984) 45; M.V. Berry and M. Wilkinson, Proc. R. Soc. Lond. **A392** (1984) 15.

[12] E. Teller, J. Phys. Chem. **41** (1937) 109.

[13] R.S. Nikam, P. Ring and L.F. Canto, Z. Phys. **A234** (1986) 241; Phys. Letters **B185** (1987) 269.

[14] Y. Sun, P. Ring and R.S. Nikam, Z. Phys. **A339** (1991) 51; R. Bengtsson, I. Hamamoto and B. Mottelson, Phys. Lett. **B73** (1978) 259; M.J.A. de Voigt, J. Dudek and Z. Szymanski, Rev. Mod. Phys. **55** (1983) 949.

[15] K. Ieki *et al.*, preprint MSUCL-851 and Phys. Rev. Lett. to be published